ELSEVIER

Surface Science 495 (2001) 77–90

SURFACE SCIENCE

www.elsevier.com/locate/susc

Universal expression for blocking cone size based on the ZBL potential

A. Kutana, I.L. Bolotin, J.W. Rabalais *

Department of Chemistry, University of Houston, Houston TX 77204-5641, USA

Received 25 April 2001; accepted for publication 13 August 2001

Abstract

Calculations of blocking cone sizes for the "blocking geometry" of the scattering and recoiling imaging spectrometry (SARIS) technique have been performed. By fitting calculated points in the space of the parameters of the interacting atomic species, a universal formula for calculating the blocking cone size for arbitrary energies and interacting species has been derived. This provides a "blocking cross-section" and an estimate of the total scattering cross-section of the process under consideration. The results obtained from the formula are compared with experimental SARIS blocking cone data for He^+ and Ne^+ scattering from a Pt(1 1 1) surface in the energy range 3–20 keV. The blocking cones in this low-energy range are appreciably asymmetric with respect to the interatomic axis. At small interatomic distances and low-projectile energies, the difference in angular size of the upper and lower halves of the blocking cone can be as large as 15%. The results of scattering and recoiling imaging code simulations and molecular dynamics blocking cone trajectory simulations using the Ziegler–Biersack–Littmark potential are in good agreement with experimental blocking cone sizes. Comparison is also made to the results of other formulas for the critical blocking angle found in the literature.

Keywords: Low energy ion scattering (LEIS); Computer simulations

1. Introduction

The effects of shadowing and blocking in medium- and high-energy ion scattering and in channeling of energetic ions in solids have been extensively studied. The origin of the shadowing and blocking concepts as related to low-energy ion scattering (LEIS) can be traced back to these studies, however they are different due to the much shorter penetration range of the particles [1]. Typical LEIS interactions with solids involve only 1–3 collisions, compared to many collisions in medium- and high-energy ion scattering. As a result, LEIS is sensitive to only the top few atomic layers of a solid and the shadowing and blocking phenomena can be used for studying the composition and structure of these top few monolayers.

A number of model investigations using shadowing/blocking cone shapes for interpretation of experimental ion scattering data have been performed [2–16]. Shadowing and channeling have been thoroughly studied since they play a major role in nearly all high-energy scattering experiments. Blocking effects are frequently studied

* Corresponding author. Tel.: +1-713-743-2701; fax: +1-713-743-2709.

E-mail address: rabalais@jetson.uh.edu (J.W. Rabalais).

0039-6028/01/$ - see front matter
PII: S0039-6028(01)01511-4

together with channeling, and many authors used these terms interchangeably. On the other hand, in many LEIS experiments, a short range blocking phenomenon is manifested that is not accompanied with channeling or shadowing as in high-energy experiments. It involves only one large angle scattering and subsequent small-angle deflection by a blocking atom. This important phenomenon in the analysis of surface structure based on "pure" blocking effects has not drawn much attention.

Most of the earlier calculations of shadowing/blocking/channeling effects [2,4,5,17,18] used semi-analytical techniques, employing an impulse approximation and/or a small-angle approximation due to limits imposed by computing powers of the times. An analytical expression for the shadow cone radius using an inverse-power potential in those approximations was obtained by Lindhard [17]. The fitting expression for the case of a more realistic screened Coulomb potential has been given by Oen [2]. It was shown by comparison to exact calculations [3] that the universal expression for the shadow cone radius obtained by Oen [2] is very good in the range of interatomic distances $\geqslant 2$ Å encountered in LEIS. In another series of works, the cross-sections for shadowing and blocking arising from a two-atom target using a backscattering geometry were generalized for arbitrary scattering angles [6] and the specific case of rainbow backscattering was studied [7]. Similar cross-section considerations were implemented to calculate intensities of direct recoils [8].

In contrast to these shadow cone calculations, no universal expression for blocking cones has been obtained. Also, there has been no direct experimental observation and quantitative interpretation of blocking cones in LEIS. Different approximations for calculation of the blocking cone size for higher energies are listed in Table 1. The observation of blocking cones in rainbow scattering at the minimum ejection angle [19] was quantified by Oen [18] using a two-atom model and, based on that description, an explicit analytic expression for the minimum exit angle in case of the inverse power interaction potential was obtained [4,5]. These calculations of the minimum ejection angle [4,5] used the small-angle approximation and assumed a monoenergetic isotropic source of scattered particles as the position of the first atom. In reality, the particles scattered by the first atom do not originate from a single fixed

Table 1
Comparison of various models used for the calculation of the blocking/critical angle

Model	Potential	BCA	Small angle approximation	Source[a]	Energy	Temperature	In-plane
String[b]	Chain[c]	N/A	N/A	Point	keV–MeV	No	Yes
Atomic chain[d]	Chain[e]	N/A	N/A	Point (recoil)	Few MeV	Yes	Yes
Two-atom[f]	$1/r^2$	Yes	Yes	From d.c.a.[g]	10 keV	Yes	Yes
Chain made of two-atom elements[h]	$1/r^n$	Yes	Yes	From d.c.a.[g]	keV	No	Yes
Two-atom[i]	$1/r^n$	Yes	Yes	Point	Tens of keV	No	Yes
Two-atom[j]	ZBL	No	No	Exact simulation	keV	No	Yes

[a] The origin of scattered particles after the first collision.
[b] Ref. [35].
[c] Based on Thomas–Fermi potential.
[d] Ref. [20].
[e] Based on Bohr potential.
[f] Ref. [13].
[g] Distance of closest approach.
[h] Ref. [4].
[i] Ref. [5].
[j] Present work.

point and particles scattered at different angles have different energies. Most importantly, the inverse-power potential is too long-ranging and a screened Coulomb potential should be used. Another formalism [20], employing the Bohr potential for the interaction of a particle with an atomic chain, was used for finding the angular size of the blocking "dip" observed in MeV ion scattering.

Facing the problem of obtaining a realistic blocking cone size and position to compare with scattering and recoiling imaging spectrometry (SARIS) measurements [21], a molecular dynamics (MD) trajectory simulation code for calculation of the critical takeoff angle has been created. Blocking cones are observed directly in SARIS [22] and their sizes can be measured experimentally. An initial attempt to find the blocking cone size dependencies on energy E and interatomic distance d has been made [22] and, from fitting of the measured dependencies for He $\rightarrow$ Pt, the power functions $d^{0.72\pm0.01}$ and $E^{0.26\pm0.01}$ were obtained. The scattering angles ($\sim$90°) used in the SARIS blocking cone observations are not close to either forward scattering or backscattering angles, which makes direct simulations more favorable for this type of measurement. In direct trajectory simulations, no simplifying assumptions about scattering angles or positions of the particles are made. In particular, the correct spatial and energy distributions of particles scattered by the first atom in the target (source) is obtained automatically.

Here we present a blocking cone size calculation for a screened Coulomb potential. We find the trajectory of the particle (projectile) in a field created by two target atoms, assuming the Ziegler–Biersack–Littmark (ZBL) interaction potential [23] and neglecting the interaction between the target particles. The parallel beam of particles having the same energy but varying impact parameter with the first atom is scattered from the target. Using a minimum exit angle search algorithm, we single out the trajectory responsible for the blocking cone formation, i.e. the envelope of the blocking cone. After fitting the calculated data, we obtain a universal formula for the blocking cone size. Finally, we compare our exact calculations with other known expressions for the minimum exit angle in the blocking geometry.

2. Methods

2.1. Experimental techniques

The measurements were carried out in a SARIS spectrometer that has been described elsewhere [22,24]. Briefly, a pulsed rare gas ion beam [25] impinging on a surface scatters and recoils atoms from the surface. The velocities of the keV ejected atoms are analyzed by measuring their flight times from the sample to a 7.5×9.5 cm^2 rectangular position-sensitive microchannel plate (MCP) detector [26] (TOF drift distance $\sim$15 cm). The MCP is mounted on a triple-axis goniometer [27] so that it can be positioned at different angles relative to the sample surface. The detector is gated so that it can be activated in windows of several μs duration that are appropriate for collection of specific scattered or recoiled atoms. Each window can be resolved into 255 time frames, which can be as short as 10 ns each. The sample is mounted on a conventional manipulator that provides reproducible rotation in both azimuthal δ and incident α angles to $\pm1°$. Good statistics are obtained with a non-destructive ion dose of $<10^{13}$ ions/cm^2. Since most of these scattered particles are neutral [28], the term "atoms" is used instead of "ions"; the MCP detector has equal sensitivity to both of these when their energies are $>$1000 eV. The pulsed, mass-selected ion beam [25] has a duoplasmotron ion source that produces beam spot sizes down to 1 mm^2 with energies variable over the range 3–25 keV and a final energy spread of $<$50 eV. A two step pulsing system produces pulsed beam widths $<$30 ns and an average beam current of 10–100 pA (0.1–1 μA dc current before pulsing). Countdown circuitry permits pulse repetition rates over a range of 5–20 kHz.

The Pt single crystal in the form of a disk 1×9 mm was polished within 0.5° of the [1 1 1] direction and cleaned by repeated cycles of 3 keV Ar^+ sputtering and annealing to 900 °C. Annealing was accomplished by electron bombardment heating from behind the crystal. The surfaces were considered clean and well ordered when no impurity features were observed in the SARIS images and the LEED images exhibited sharp (1×1) patterns.

The scattering experiments reported herein were carried out in a subsurface-sensitive backscattering or "blocking configuration" [22] that uses large scattering ($\theta = 70$–$135°$) and exit ($\psi = 25$–$100°$) angles. In such a geometry, the features of the SARIS images are determined by the atomic trajectories that result from large-angle scattering events with subsurface atoms and blocking and focusing of these trajectories by atoms in layers nearer to the surface.

2.2. Trajectory simulations

Interpretation of the images has been described elsewhere [22] and was facilitated by computer simulations based on the classical theory of ion scattering [29,30] using the binary collision approximation (BCA) simulation program scattering and recoiling imaging code (SARIC) [31,32] and "two-atom" MD simulations. SARIC is based on the BCA, uses screened Coulomb potentials to describe the interactions between atoms, and follows the trajectories of all scattered and recoiled atoms in three-dimensions, thereby capturing both in- and out-of-plane single and multiple collision events. The ZBL universal potential [23] was used for these specific simulations. Details of the SARIC simulation are provided elsewhere [31,32]. The MD simulation will be described below. The power of the MD method is its simplicity, its capability of providing exact results, and the decreased computing time compared to 3D SARIC simulations.

3. Results

3.1. Molecular dynamics simulations

In order to provide additional computational support for the SARIS measurements along with a more routine analysis of SARIS frames, an MD program was developed to calculate the sizes of blocking cones formed by scattering a parallel beam of projectiles from a two-atom target by consecutive scattering from the first and second atoms. The studied system is shown in Fig. 1a and consists of two atoms separated by a distance d. When a beam of ions with parallel trajectories interacts with atom 1 (scattering atom), the latter acts as a source of scattered particles with a near isotropic angular distribution. The position of the source is displaced a very small distance $\rho \sim 0.1$ Å from atom 1. Some of these trajectories are deflected by the repulsive potential of atom 2 (blocking atom). This results in a hyperboloid-like "blocking cone" with apex on atom 1 and centered approximately on the interatomic axis. It is necessary to determine the critical blocking angle ψ_c when atom 2 begins to block the scattered trajectories from atom 1.

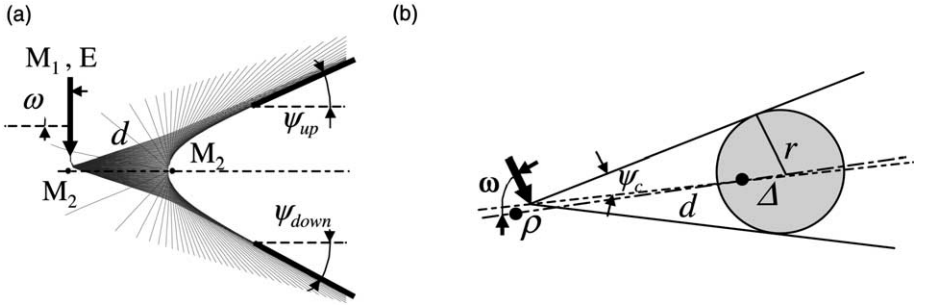

Fig. 1. Systems of two atoms with interatomic distance d. (a) MD trajectory simulation for the same system showing the blocking cone formation. The parallel beam of particles of energy E and mass M_1 is incident on two atoms of mass M_2. There are two critical scattering angles ψ_{up} and ψ_{down} on both sides of the interatomic axis. The critical blocking angle ψ_c is defined as $\psi_c = 1/2(\psi_{up} + \psi_{down})$. (b) Emission from the secondary point source of scattered particles at a distance ρ from atom 1 is blocked by atom 2. The blocking effect of the second atom is represented by a geometrical optics shadow behind a hard sphere of radius r at a distance d from the atom. The critical blocking angle $\psi_c \approx \arcsin(r/d + \Delta)$ is indicated.

Ion trajectories, critical angles with corresponding impact parameters (p) with the first atom, and differential scattering cross-sections were calculated for this system. As an example, the simulated dependence of the exit angle for 10 keV He^+ impinging on two Pt atoms separated by 5 Å as a function of p with the first Pt atom is shown in Fig. 2 (solid dots). The critical blocking angles above and below the interatomic axis are ψ_{up} and ψ_{down}, with corresponding p_{up} and p_{down}. The dashed line corresponds to the calculation for a system with the second atom removed. The inset shows the differential scattering cross-section $\sigma_{d\Omega} = p((d\psi/dp)\sin\psi)^{-1}$ versus the exit angle with respect to the interatomic axis ψ for the two-atom (solid line) and one-atom (dashed line) targets. The area under each curve is preserved and corresponds to the flux of particles scattered into the $-20°$ to $+20°$ angle range.

The purpose of the MD simulation is to find the two minimum in-plane projectile exit angles ψ_{up} and ψ_{down} on both sides of the interatomic axis whose sum $\psi_{up} + \psi_{down}$ yields the size of the blocking cone (Fig. 1a). In order to follow the

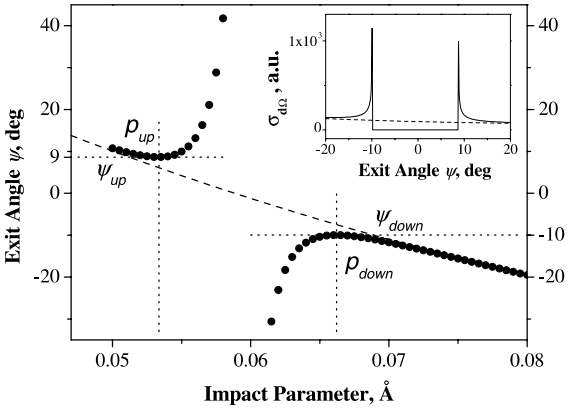

Fig. 2. (dots) MD simulation of the dependence of the exit angle for 10 keV He^+ impinging on two Pt atoms separated by 5 Å as a function of impact parameter p with the first Pt atom. The critical blocking angles above and below the interatomic axis ψ_{up} and ψ_{down} and the corresponding projectile impact parameters p with the first atom p_{up} and p_{down} are indicated. (dashed line) Calculation for a system with the second atom removed. (inset) The differential scattering cross-section versus exit angle for two-atom (solid line) and one-atom (dashed line) targets. The area under each curve is preserved and corresponds to the flux of particles scattered into the $-20°$ to $+20°$ range.

trajectories of the particles, the Newtonian equations of motion were numerically solved using a fourth-order Runge–Kutta method [33]. The projectile and each of the target atoms were allowed to interact according to the ZBL potential and there was no interaction between the target atoms themselves. The included parameters affecting the size of the blocking cone are: mass ratios and atomic numbers of projectile and target atoms, interatomic distance d, primary energy of projectile E, and "incident angle" ω, defined as the angle between the incident beam and interatomic axis in the direction from the first to the second atom. The angles of incidence are large enough (from 70° to 120°) to allow projection of scattered particles both above and below the second atom. In-plane quasi-single scattering trajectories that described the two halves (upper and lower) of a blocking cone were calculated. The trajectory of the projectile which, after being scattered with all possible impact parameters from atom 1 towards atom 2, would have the minimal exit angle, contributes to the envelope of the blocking cone. In order to find such trajectory for each side of the blocking cone, the projectile was directed at atom 1 with p corresponding to the two values of the single scattering angle θ_1. For example, for the upper side, the first value of θ_1 chosen was slightly greater than the projectile incidence angle ω in order to direct the projectile almost head-on at the second atom. This corresponds to the large value of the total scattering angle due to atom 2. The second value of θ_1 was chosen large enough to ensure a large total scattering angle mostly due to atom 1 and almost no interaction with atom 2. The smallest value of the total scattering angle corresponding to the upper half-size of the blocking cone lies somewhere between these two limiting values. This minimum value was found using the golden section minimum search algorithm for a one-variable function [34].

The critical blocking angle $\psi_c = 1/2(\psi_{up} + \psi_{down})$ when atom 2 begins to block the trajectories scattered from atom 1 so that the total scattering angle starts to increase again was determined. Contrary to the case of a monoenergetic "point emitter" source [5,20,35], when a real atom serves as a source of particles, $\psi_{up} \neq \psi_{down}$ and, therefore, the

center of the blocking cone does not correspond to the interatomic axis direction. The analysis was conducted in two dimensions since it was computationally expensive to realize a machine algorithm for finding a blocking cone size in three dimensions. No temperature effects have been taken into consideration in this calculation. It is known from SARIC calculations [22] that introducing atomic vibrations causes blurring of the blocking cone edges leading to larger blocking cone sizes. This fact has been accounted for in experiment by taking the ψ_c value at 70% of the maximum intensity near the edge of the blocking cone.

3.2. Blocking cross-section

Experimental SARIS frames for 5–20 keV He^+ and 20 keV Ne^+ scattering from a clean Pt(1 1 1) surface in the [2 1 1] blocking direction are shown in Fig. 3. Each frame represents the velocity-resolved spatial distributions of He or Ne atoms scattered along different angles and arriving at the MCP in a window of 16.7 ns duration. The frames were selected to correspond to the flight time of quasi-single scattered He or Ne atoms, e.g. at ~0.15 μs for 20 keV He, from Pt. The ordinate of each frame is the particle exit angle (β) from the surface and the abscissa is the crystal azimuthal angle (δ), i.e. each frame is an image in β, δ-space. The δ angles are defined with respect to the [1 $\bar{2}$ 1] azimuth. Since the MCP is planar rather than spherical, the lines of constant azimuthal angle and constant exit angle are not linear and the values of β and δ on Fig. 3 serve only as guides. If the incident ions interact with only individual atoms, blocking cones or high-intensity "rings" due to trajectory focusing are observable. When the ions interact simultaneously with a group of atoms in an ordered arrangement, e.g. an atomic lens [36], intense focusing spots or streaks can be produced as observed in Fig. 3. Examples of SARIS frames for other blocking directions are presented elsewhere [22].

The table in Fig. 3 lists the sizes of the ψ_c angles for the Pt(1 1 1)-[2 1 1] blocking cones measured by the SARIS method described elsewhere [22]. Briefly, the cones intersect the plane of the detector as ellipses (Fig. 3) with semi-major (a_e) and semi-minor (b_e) axes. The sizes of ellipses are defined as the angular aperture corresponding to the position of 70% of the maximum scattered intensity at the cone edges. This criterion has been chosen using the condition of equality of blocking cone sizes in SARIC simulations for a given target at $T = 0$ and 300 K. Finally, the blocking cone size is defined from the expression

$$\tan(\psi_c) = \frac{b_e^2}{a_e h}, \quad (1)$$

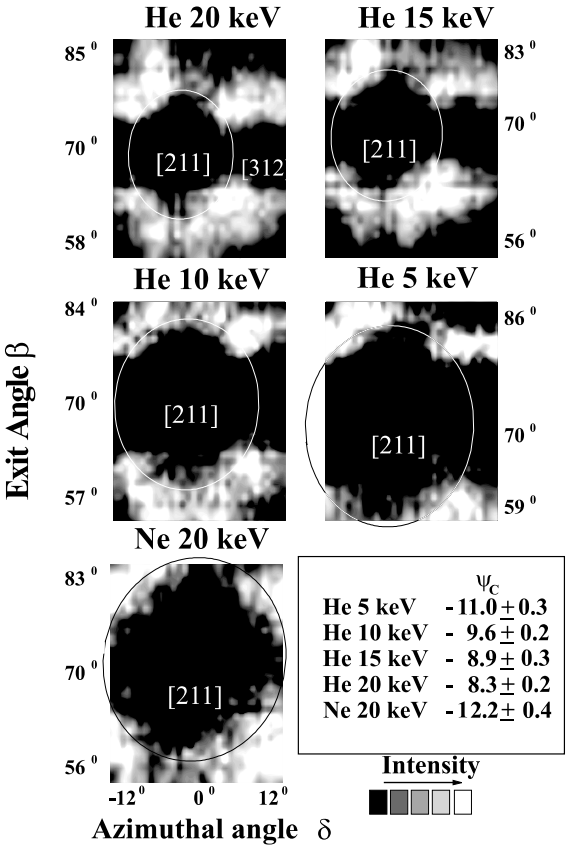

Fig. 3. Experimental SARIS frames in β, δ- space in the crystallographic [2 1 1] direction for scattering of 5–20 keV He^+ and 20 keV Ne^+ from Pt(1 1 1) with incident angles in the range 30–35°. The δ angles are defined with respect to the [1 $\bar{2}$ 1] azimuth. Planar backgrounds have been subtracted from the images and different intensity scales are used for each image in order to best emphasize the blocking phenomena. Ellipses designating shapes of blocking cones are drawn at 70% of the intensity. The table lists the sizes of observed ψ_c blocking cone angles.

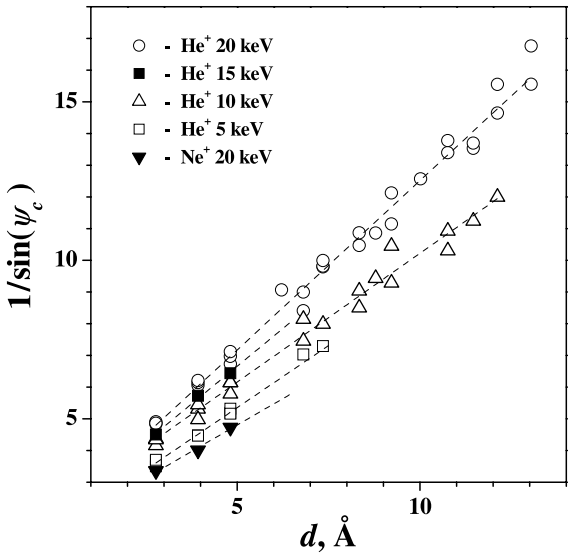

Fig. 4. (symbols) Relative sizes of experimental blocking cones from the experimental SARIS images as a function of the interatomic distance d for different He^+ and Ne^+ energies. (dashed lines) Least-squares line fits to the experimental points.

Table 2
Results of linear fitting of experimental data along with SARIC and MD calculations used for determination of the blocking cross-section σ

	r (Å)	Δ (Å)	$\sigma = \pi r^2$ (Å^2)
He (20 keV)			
Experiment	0.94 ± 0.04	1.7 ± 0.5	2.8 ± 0.1
SARIC	1.07 ± 0.03	2.6 ± 0.3	3.6 ± 0.1
MD	1.01 ± 0.01	2.40 ± 0.07	3.20 ± 0.03
He (15 keV)			
Experiment	1.05 ± 0.08	2.0 ± 0.5	3.5 ± 0.3
MD	1.08 ± 0.01	2.31 ± 0.07	3.66 ± 0.03
He (10 keV)			
Experiment	1.20 ± 0.04	2.4 ± 0.5	4.5 ± 0.2
SARIC	1.31 ± 0.03	3.0 ± 0.2	5.4 ± 0.1
MD	1.18 ± 0.01	2.20 ± 0.07	4.37 ± 0.04
He (5 keV)			
Experiment	1.28 ± 0.06	1.8 ± 0.4	5.1 ± 0.2
SARIC	1.49 ± 0.04	2.8 ± 0.3	7.0 ± 0.2
MD	1.37 ± 0.01	2.01 ± 0.06	5.90 ± 0.04
Ne (20 keV)			
Experiment	1.5 ± 0.1	2.2 ± 0.6	7.1 ± 0.5
MD	1.38 ± 0.01	1.86 ± 0.06	5.98 ± 0.04

where h is the distance from the detector plane to sample. The sizes of the experimental blocking cones as a function of the interatomic distance d for different energies are shown in Fig. 4. If these sizes are plotted as $1/\sin(\psi_c)$ versus d, the dependencies are nearly linear as shown by dashed lines in Fig. 4. Such linear dependencies allow determination of a "blocking cross-section".

If the blocking due to atom 2 is approximated as a geometrical optics-like shadow behind a sphere with radius r placed at a distance a from atom 1 (Fig. 1b), it is easy to see that

$$1/\sin(\psi_c) \approx \frac{a}{r}. \quad (2)$$

In a simple approximation $a \approx d + \Delta$, therefore the slope of the linear dependence $1/\sin(\psi_c)$ vs. d gives the value of r. In this case the total scattering cross-section of the second atom, or blocking cross-section is equal to πr^2. Table 2 summarizes the results of such linear fitting of the experimental data.

This simple empirical two-atom model for blocking cone analysis was tested by performing SARIC and MD calculations for an isolated system of two atoms using different He^+ and Ne^+ energies as shown in Figs. 5 and 6. The results for each energy value exhibit nearly linear dependencies versus interatomic spacing. Linear fittings of SARIC and MD calculations are also presented in Table 2. The expressions obtained are in excellent agreement with the experimental results of Fig. 4. We note that MD simulations give better agreement with experimental values than SARIC simulations. This results from the fact that correlated scattering events are treated more precisely by exact MD trajectory simulations than the BCA. Also, from the calculated curves we note that the dependencies depart from linearity as d decreases, although these deviations are beyond our experimental resolution.

3.3. Universal formula for blocking cone size from MD simulations

The simple geometrical optics analogy for blocking cone formation by a second atom described

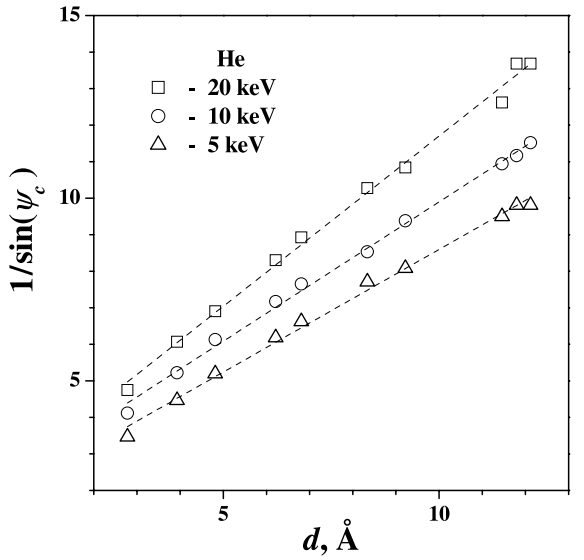

Fig. 5. (symbols) SARIC BCA simulations of the relative sizes of the blocking cones as a function of interatomic distance d for a two-atom target at $T = 0$ K for He^+ projectiles at three different energies with incident beam angle $\omega = 110°$. (dashed lines) Best fit line to the simulated points.

in Section 3.2 gives only an estimate of the measured blocking cone sizes. In order to determine accurate blocking cone sizes for any interacting atomic pairs, energies, and angles, more exact calculations are necessary. The procedure for obtaining a universal formula for the blocking cone size will now be developed. Fig. 6(b) shows a plot of $\log\psi_c$ versus $\log d$ for He and Ne at various energies scattered from Pt with an $\omega = 90°$ incidence angle. Similar near linear dependencies are found in the $\log\psi_c$ versus $\log E$ plots for various d (not shown here). The critical blocking angles are determined as $\psi_c = 1/2(\psi_{up} + \psi_{down})$, where $\psi_{down} = k\psi_{up}$ with $k \geqslant 1$. In a first approximation, $k \approx 1$ so that $\psi_{down} \approx \psi_{up}$, and $\psi_c \approx \psi_{up}$. As a result, the calculated values of ψ_{up} can be fitted with a second-order surface $z = z(x, y)$, as shown in Fig. 7, with $x = \ln(d)$, $y = \ln(E)$, and $z = \ln(\psi_{up})$, where E is the projectile energy in keV and d is the distance between the target atoms in Å. The blocking cone sizes found for various parameters $(M_1, M_2, Z_1, Z_2, \omega)$ are fitted with a formula analogous to the one derived for the inverse-power potential [5,22],

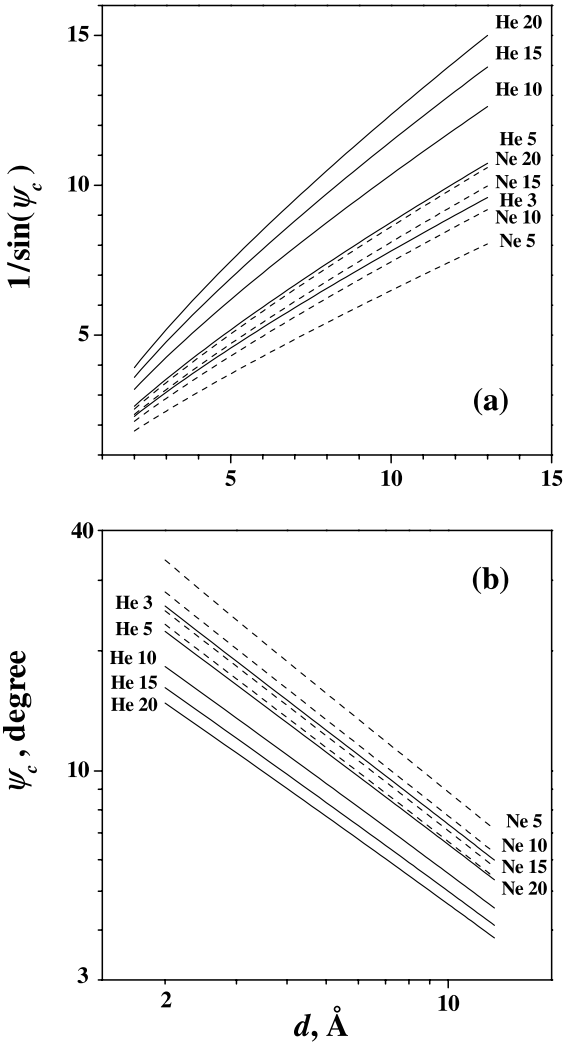

Fig. 6. MD simulations of blocking cone sizes as a function of interatomic distance d for the same two-atom target used in Fig. 5 for five He (solid lines) and four Ne (dashed lines) energies. (a) Relative sizes of blocking cones. (b) Sizes of blocking cones on a logarithmic scale. The numbers to the right of the elemental symbols represent their kinetic energy in keV.

$$\psi_{up} = Dd^{-n}E^{-m}, \tag{3}$$

but here D, n, and m are now functions of the five parameters $(M_1, M_2, Z_1, Z_2, \omega)$. Not all of these parameters are independent, as follows from the properties of the equations of motion and form of the potential function.

Due to the invariance of the equations of motion with respect to the transformation $M_i \to kM_i$,

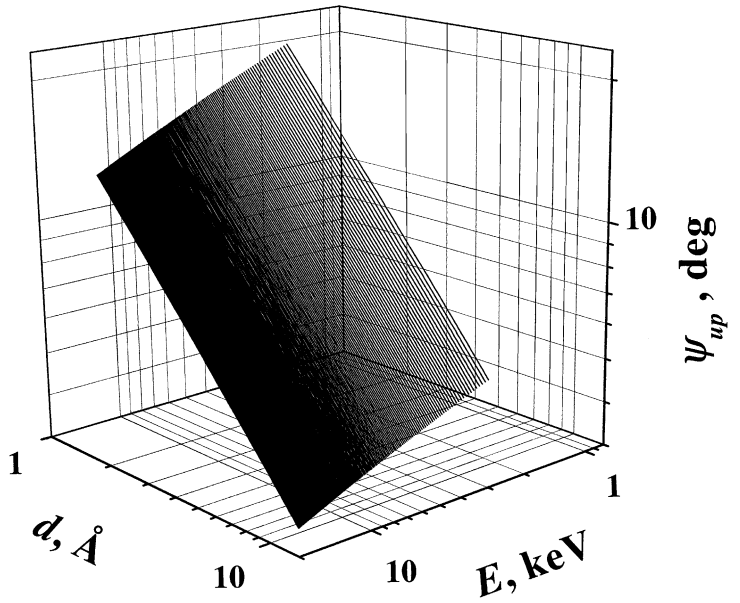

Fig. 7. Example of a second order surface in $\ln(d)$, $\ln(E)$, and $\ln(\psi_{up})$ space for the He^+–Pt combination used in the universal fitting.

$t \to t/\sqrt{k}$ (see Appendix A), where M_i are the masses of interacting particles and t is time, the trajectory shape is the same for the combinations of particles connected via Eq. (A.2) provided that the particles have the same initial energies. Therefore, there is only one independent variable in the set (M_1, M_2), namely, the ratio M_1/M_2. It is possible to reduce the number of independent parameters in the set (Z_1, Z_2) by finding their combinations based on the following. The screened ZBL potential is a product of a "Coulomb" term containing Z_1Z_2 and a screening function containing $(Z_1^{0.23} + Z_2^{0.23})$ [23]. In general, both of these terms should be incorporated into the fitting expression. We find that the $\ln(Z_1Z_2)$ term is most important in the "energy" term m and pre-exponential term D while the $(Z_1^{0.23} + Z_2^{0.23})$ term is most important in the "distance" term n. As a result, we can write:

$$\begin{aligned} \ln(D) &= f\left(\frac{M_1}{M_2}, \ln(Z_1Z_2), \ln(\omega)\right), \\ n &= n\left(\frac{M_1}{M_2}, Z_1^{0.23} + Z_2^{0.23}, \ln(\omega)\right), \\ m &= m\left(\frac{M_1}{M_2}, \ln(Z_1Z_2), \ln(\omega)\right). \end{aligned} \tag{4}$$

After fitting $\ln(\psi_{up}) = z$ (Fig. 7) with a second-order surface in x and y $(z = F_0 + F_1x + F_2x^2 + F_3xy + F_4y + F_5y^2)$ for a fixed set of $(M_1/M_2; Z_1, Z_2; \omega)$, six values of F_i in $(M_1/M_2; Z_1, Z_2; \omega)$ space are obtained. It was possible to fit the calculated points for 120 projectile–target combinations by a hyperplane in $[M_1/M_2, \ln(Z_1Z_2), \ln(\omega)]$ space for four of the coefficients (F_0, F_3, F_4, F_5) of decomposition of $\ln(\psi_{up})$ in x and y and in $[M_1/M_2, Z_1^{0.23} + Z_2^{0.23}, \ln(\omega)]$ space for the other two (F_1 and F_2). The range of target interatomic distances used in the calculations was $d = 2$–13 Å, the energy range was $E = 3$–20 keV, the ω range was 70–125°, the M_1/M_2 range was 0–0.33, and the product Z_1Z_2 varied between 40 and 1600. The final fitting expression for finding ψ_{up} is

$$\psi_{up} = \exp\left(F_0 + F_1x + F_2x^2 + F_3xy + F_4y + F_5y^2\right), \tag{5}$$

where

$$F_i = f_i + h_i\frac{M_1}{M_2} + g_i\ln(Z_1Z_2) + e_i\ln(\omega) \tag{6a}$$

for $i = 0$, 3–5, and

Table 3
Numerical values of parameters in Eqs. (6a) and (6b) found from fitting MD calculations of the blocking cone size (ψ_{up})

	0	1	2	3	4	5
f_i	1.34 ± 0.04	0.13 ± 0.03	-0.074 ± 0.003	-0.060 ± 0.004	0.0096 ± 0.0009	-0.0404 ± 0.0009
h_i	0.90 ± 0.01	-0.24 ± 0.01	0.0255 ± 0.0006	0.0084 ± 0.0008	0.047 ± 0.002	-0.0010 ± 0.0001
g_i	0.174 ± 0.001	-0.133 ± 0.003	0.0093 ± 0.0002	0.0043 ± 0.0001	0.0167 ± 0.0004	0.00253 ± 0.00003
e_i	0.36 ± 0.01	-0.078 ± 0.007	0.0053 ± 0.0005	0.0140 ± 0.0009	-0.069 ± 0.003	0.0032 ± 0.0002

Table 4
Numerical values of parameters in Eq. (7) for finding the coefficient k used in determining the size of the lower part of the blocking cone for four common systems. In all calculations, $\omega = 90°$

	F'_0	F'_1	F'_2	F'_3	F'_4	F'_5
He–Pt	0.4578 ± 0.0002	-0.1075 ± 0.0001	0.00945 ± 0.00003	0.01535 ± 0.00003	-0.1085 ± 0.0002	0.00510 ± 0.00003
Ne–Pt	0.1749 ± 0.0001	-0.1941 ± 0.0001	0.0212 ± 0.0002	0.0253 ± 0.0002	-0.1653 ± 0.0009	0.0077 ± 0.0002
Ne–Ni	0.2341 ± 0.0002	0.0042 ± 0.0001	-0.00536 ± 0.00002	0.01017 ± 0.00003	-0.0980 ± 0.0001	0.00481 ± 0.00002
He–Si	0.1494 ± 0.0001	-0.0150 ± 0.0001	-0.00051 ± 0.00001	0.00667 ± 0.00001	-0.0747 ± 0.0001	0.00800 ± 0.00001

$$F_i = f_i + h_i \frac{M_1}{M_2} + g_i\left(Z_1^{0.23} + Z_2^{0.23}\right) + e_i \ln(\omega) \qquad (6b)$$

for $i = 1$, 2. The numerical values of the coefficients f_i–e_i are given in Table 3. The values of ψ_{up} found using Eq. (5) are within 0.5° of the exact values obtained from MD simulations. The lower part of the blocking cone can be estimated from $\psi_{down} = k\psi_{up}$, where k is in the range 1.0–1.3 and is dependent on the same variables as ψ_{up}. We do not provide a universal fitting formula for ψ_{down} here since its fitting coefficients represent surfaces whose analytical forms in the space of the parameters are not that straightforwardly determinable as in case of ψ_{up}. Table 4 presents the fitting coefficients F'_0–F'_5 of the expression

$$\ln k = F'_0 + F'_1 \ln d + F'_2 (\ln d)^2 + F'_3 \ln d \ln E + F'_4 \ln E + F'_5 (\ln E)^2 \qquad (7)$$

for the case of four projectile–target combinations.

4. Discussion

4.1. Comparison of BCA and MD simulations

Accurate calculations of blocking cone sizes are important when using SARIS and other ion scattering experiments for surface composition and structure determination. A correct description of blocking cone sizes in SARIS experiments requires essentially exact calculations of the scattering trajectories. The reason for this is that large scattering angles, i.e. ~90°, are used in these types of experiments. This is different from the case of shadow cone calculations where, due to the small scattering angles, momentum and small angle approximations give satisfactory results. Another reason for using trajectory simulations when determining blocking cone size is that due to the number of atoms encountered along the trajectory, correlational effects must be taken into account. The BCA [37] treats this problem reasonably well when asymptote displacements are small compared to interatomic distances. Our comparison (Table 2) of MD trajectory simulations with SARIC BCA calculations shows that use of the BCA approximation leads to slightly larger (~18%) blocking cross-sections. A simplifying assumption in the BCA is that the energy and direction of a particle is changed instantaneously as it proceeds along its trajectory at certain positions in space where the collisions are assumed to take place. In MD calculations, the energy of the particle changes continuously along the trajectory. For a two-atom target, this simplifying assumption may lead to the

fact that the impact parameter with the second atom is slightly greater than in MD simulations. Unlike Oen's shadow cone calculations [2], in blocking cone calculations it does not seem possible to find a combination of parameters as one universal variable for blocking cone size dependence.

Our calculations show that the more accurate MD simulations reveal the asymmetry in the blocking cone size with respect to the interatomic axis. For small d and E, the asymmetry of the blocking cone $\gamma = \psi_{\text{down}} - \psi_{\text{up}}$ is maximum and decreases with increasing d and E. This is important in the low-energy range when the critical angles are large and the displacements of the "virtual source" from the first atom cannot be neglected. We note that although in the double alignment experiments in the RBS technique this asymmetry is small enough to be neglected [9], care must be taken in LEIS when drawing conclusions about surface relaxation based on the shape of the blocking cone.

Our consideration is limited to only the case of $T = 0$, or, in other words, temperature is not a part of the model. The case of $T \neq 0$ requires the use of a statistical model, of which our deterministic model is a limiting case. In the framework of a statistical model, an average quantity corresponding to the deterministic blocking cone size can be introduced. Presently, it is not clear how our model could be generalized to include target vibrations. In principle, one could obtain the probability distribution of the blocking cone sizes for a given amplitude of target vibrations, but this would mean an increase in computational time of several orders of magnitude, which is already a critical factor. Instead, we extrapolate the experimental blocking cone sizes to the case $T = 0$, where they can be compared to our calculations.

4.2. Comparison to other published results

The results of our fitting formula for the blocking cone sizes are compared with the experimental SARIS cones and other blocking cone expressions found in the literature (see Fig. 8 and Table 1). The subject has been widely discussed in high-energy ion scattering where the formulas are most accurate. The sizes of the observed blocking dips are about one order of magnitude less than the sizes of the SARIS blocking cones. These formulas do not give accurate blocking cone sizes for our low-energy region.

The first and simplest theory of the blocking effect was given by Oen [18] for explanation of the observed dip in the intensity of α-particles scattered in the $\langle 1\,1\,1\rangle$ direction from W bombarded by 60 keV $^{222}\text{Rn}^{+}$ [19]. It was assumed that the source of α-particles was at a position of a target atom and blocking was due to the nearest atom in the $\langle 1\,1\,1\rangle$ direction. The scattering intensity was calculated but an explicit formula for ψ_c was not provided. Martynenko [4] and Mashkova and Molchanov [5] derived the following expression for the minimum exit angle for case of a A/r^s potential as

$$\psi_{\min} = \left(1 + \frac{1}{s}\right)\left(\frac{sA\sqrt{\pi}}{Ed^s}\,\frac{\Gamma\left(\frac{s+1}{2}\right)}{\Gamma\left(\frac{s}{2}\right)}\right)^{1/(s+1)}, \tag{8}$$

where $A = 0.831 Z_1 Z_2 e^2 a_L^{s-1}/s$, $a_L = 0.4685/(Z_1^{2/3} + Z_2^{2/3})^{1/2}$ are the constant and screening length for the form of the inverse-power potential provided by Lindhard [38], and Γ is a gamma-function. This expression was obtained for a target viewed as an atomic chain consisting of two-atom elements. The two lines calculated with this formula for inverse-square and inverse-cube potentials are shown in Fig. 8. The A/r^3-type potential yields ~53% smaller blocking cone size, although it provides the correct slope on the logarithmic scale. The correction for non-zero distance of the scattered projectile from the first atom after the first collision [4,5] was not taken into account since it further diminished the blocking cone sizes.

An analytical expression for the case of an atomic chain was provided by Lindhard as

$$\psi_c = \psi_L\left(\log\frac{4.663 C a_L}{\psi_L d}\right)^{1/2} \tag{9a}$$

for $\psi < a_L/d$, and

$$\psi_c = \left(\frac{2.828\psi_L C a_L}{d}\right)^{1/2} \tag{9b}$$

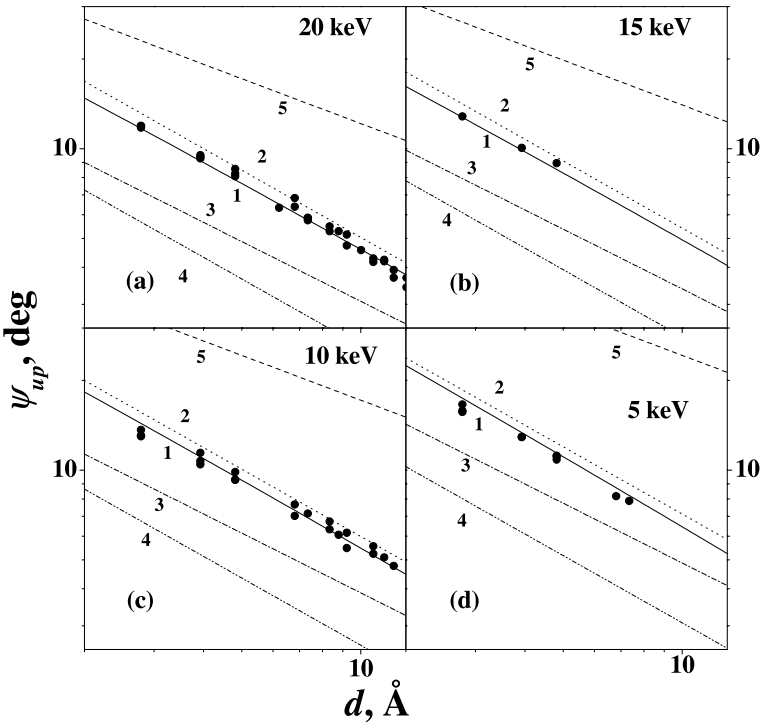

Fig. 8. Comparison of the fitting formula developed herein for the blocking cone size with experimental results and other blocking cone size expressions found in the literature for the He–Pt projectile–target combination at four different energies. Symbols–experimental SARIS data. The lines represent blocking cone sizes calculated from: (1) our fitting formulas (Eqs. (5)–(7)) with $\omega = 90°$ and coefficients from Tables 3 and 4. (2) Lindhard's formula [35]. (Eq. (9b)), (3) Inverse-power potential A/r^s (A from Lindhard [38]) for $s = 2$ [4,5]. (4) Inverse-power potential A/r^s(A from Lindhard [38]) for $s = 3$ [4,5]. (5) Tulinov et al. [20] formula.

for $\psi > a_L/d$, where $\psi_L = (2Z_1Z_2e^2/Ed)^{1/2}$ is the Lindhard critical angle and d is the interatomic distance in the chain. In our case $\psi \geqslant a_L/d$. The line for ψ_c calculated from Eq. (9a) with a fitting coefficient $C = \sqrt{3}$ as proposed by Lindhard [35] is shown in Fig. 8. The Lindhard lines are ~10% higher than our results. The modified value of the Lindhard parameter $C' = C/1.2$ gives somewhat better agreement with our formula. As observed from Fig. 8, the Lindhard curve is the closest one to the exact calculation for all analyzed energies.

In the MeV region, due to the much larger ranges of particles in solids, blocking effects are usually described as interactions of a particle with an atomic row. The angular size of the "dips" observed in such scattering experiments has been calculated [20] for interaction of a particle with an atomic chain using the Bohr potential to be

$$\psi_c^2 = 2\frac{b}{d}\left(K_0\left(\frac{\sqrt{bd}}{a_B}\right) + 2\right), \tag{10}$$

where K_0 is the modified Bessel function, $a_B = 0.529/\left(Z_1^{2/3} + Z_2^{2/3}\right)^{1/2}$ Å is the Bohr screening length, and $b = Z_1Z_2e^2/E$. This dip can be observed along any low-index crystalline direction where atoms in the crystal are "lined up" and are closely spaced. The typical size of a dip for these energies ranges from a fraction of a degree to several degrees. The size of the blocking cone calculated from this formula for keV He → Pt gives values of ψ_c that are 2.5–3.5 times larger (Fig. 8) than our experiment and calculation.

As shown in Fig. 8, our fitting formula provides the best agreement with the experimental data. If the constants in Eqs. (8), (9a) and (9b) are modi-

fied, they can be made more suitable for our energy range.

5. Conclusions

The expression developed herein for calculation of blocking cone sizes in LEIS (3–20 keV) has been successfully applied to interpretation of SARIS experimental data. The expression was developed by fitting data points produced by MD trajectory simulations with a ZBL potential for 120 atomic collision pairs. In observations of blocking cones in the SARIS experiment, the effect of the blocking atom is closely approximated by that of a hard sphere of constant radius if the energy and interacting species are fixed. The cross-section of the sphere, πr^2, with $r \sim 1$ Å, is called the blocking cross-section. This value provides an estimate of the total scattering cross-section of the process under consideration. The blocking cones in this low energy range are appreciably asymmetric with respect to the interatomic axis, with the "lower" part being larger than the "upper" part. At small interatomic distances and low projectile energies, the difference in the blocking cone sizes can be as large as 15%. The results of the MD blocking cone size simulations using the ZBL potential and SARIC simulations are in good agreement with experimental blocking cone sizes. Finally, comparison with the various expressions for the blocking cone size found in the literature has been performed. The best agreement is with the Lindhard formula and the A/r^3-type potential, if the constants C and A from these formulas are modified.

Acknowledgements

This material is based on work supported by the National Science Foundation under grant no. CHE-998607.

Appendix A

In the Lagrangian equations of motion

$$\frac{\partial}{\partial t}(M_i\dot{q}_i) + \frac{\partial V}{\partial q_i} = 0. \tag{A.1}$$

The transformation to a new set of masses via

$$M_i' \to kM_i, \tag{A.2}$$

where k does not depend on i, can be reduced to the transformation of the time scale

$$t' \to t/\sqrt{k}, \tag{A.3}$$

so that the equations remain unchanged in the new time variable t':

$$\frac{\partial}{\partial t'}(M_i\dot{q}_i) + \frac{\partial V}{\partial q_i} = 0 \tag{A.4}$$

If the initial energy of the projectile is kept constant, although the projectile and target masses are changing according to Eq. (A.2), these new equations will have the same solution because the projectile velocity scales as $\sqrt{k}$ with its mass scaling as k and its energy remaining unchanged. This means that in the new time variable $q_0' = q_0$ and $\dot{q}_0' = \dot{q}_0$. It follows that in order to obtain a solution for M_i' from a solution for M_i, one should decrease all the particle velocities by a factor of $\sqrt{k}$ and leave the trajectories unchanged. For our analysis, this means that the blocking cone size depends on the ratio M_1/M_2 and not on M_1 and M_2 independently.

References

[1] J.W. Rabalais, Surf. Sci. 299/300 (1994) 219.
[2] S. Oen, Surf. Sci. 131 (1983) L407.
[3] B. Hird, Can. J. Phys. 69 (1991) 70.
[4] Yu.V. Martynenko, Radiat. Eff. 20 (1973) 211.
[5] E.M. Mashkova, V.A. Molchanov, Radiat. Eff. 25 (1974) 33.
[6] R.S. Williams, M. Kato, R. Daley, M. Aono, Surf. Sci. 225 (1990) 355.
[7] R.S. Daley, D. Farrelly, R.S. Williams, Surf. Sci. 234 (1990) 355.
[8] S. Chaudhury, R.S. Williams, Surf. Sci. 255 (1991) 127.
[9] W.C. Turkenburg, W. Soszka, F.W. Saris, H.H. Kersten, B.G. Colenbrander, Nucl. Instrum. Meth. 132 (1976) 587.
[10] J.P. Biersack, L.G. Haggmark, Nucl. Instrum. Meth. 174 (1980) 257.
[11] R.M. Tromp, J.F. van der Veen, Surf. Sci. 133 (1983) 159.
[12] R.S. Daley, J.H. Huang, R.S. Williams, Surf. Sci. 215 (1989) 281.
[13] D.S. Karpuzov, Phys. Stat. Sol. 64 (1974) 351.
[14] J.F. van der veen, Surf. Sci. Rep. 5 (1985) 199.

[15] J.A. Yarmoff, D.M. Cyr, J.H. Huang, S. Kim, R.S. Williams, Phys. Rev. B 33 (1986) 3856.
[16] E. Taglauer, M. Beckschulte, R. Margraf, D. Mehl, Nucl. Instrum. Meth. B 35 (1988) 404.
[17] J. Lindhard, Phys. Lett. 12 (1964) 125.
[18] O.S. Oen, Phys. Lett. 19 (1965) 358.
[19] B. Domeji, K. Bjorkqvist, Phys. Lett. 14 (1965) 358.
[20] A.F. Tulinov, V.S. Kulikauskas, M.M. Malov, Phys. Lett. 18 (1965) 304.
[21] C. Kim, C. Hofner, A. Al-Bayati, J.W. Rabalais, Rev. Sci. Instrum. 69 (1998) 1676.
[22] I.L. Bolotin, L. Houssiau, J.W. Rabalais, J. Chem. Phys. 112 (2000) 7181.
[23] J.F. Ziegler, J.P. Biersack, U. Littmark, in: J.F. Ziegler (Ed.), The Stopping and Range of Ions in Solids, Pergamon Press, NY, 1985.
[24] C. Kim, C. Höfner, A. Al-Bayati, J.W. Rabalais, Rev. Sci. Instrum. 69 (1998) 1676.
[25] Peabody Scientific, P.O. Box 2009, Peabody, MA 01960.
[26] C. Kim, A. Al-Bayati, J.W. Rabalais, Rev. Sci. Instrum. 69 (1998) 1289.
[27] J. Yao, C. Kim, J.W. Rabalais, Rev. Sci. Instrum. 69 (1998) 306.
[28] J.W. Rabalais, CRC Crit. Rev. Solid. State Mater. Sci. 14 (1988) 319.
[29] E.S. Parilis, L.M. Kishinevsky, N.Yu. Turaev, B.E. Baklitzky, F.F. Umarov, V.Kh. Verleger, I.S. Bitensky, Atomic Collisions on Solids, North-Holland, New York, 1993.
[30] E.S. Mashkova, V.A. Molchanov, Medium-Energy Ion Reflection from Solids, North-Holland, Amsterdam, 1985.
[31] S.S. Sung, V. Bykov, A. Al-Bayati, C. Kim, S.S. Todorov, J.W. Rabalais, Scanning Microsc. 9 (1995) 321.
[32] V. Bykov, C. Kim, M.M. Sung, K.J. Boyd, S.S. Todorov, J.W. Rabalais, Nucl. Instrum. Meth. B 114 (1996) 371.
[33] W.H. Press, B.P. Flannery, S.A. Teukolsky, W.T. Vetterling, in: Numerical Recipes (FORTRAN), Cambridge University Press, Cambridge, 1989, p. 550.
[34] W.H. Press, B.P. Flannery, S.A. Teukolsky, W.T. Vetterling, in: Numerical Recipes (FORTRAN), Cambridge University Press, Cambridge, 1989, p. 277.
[35] J. Lindhard, Mat. Fys. Medd. Dan. Vidensk. Selsk. 34 (14) (1965) 1.
[36] C. Kim, J.W. Rabalais, Surf. Sci. 395 (1998) 239.
[37] M.T. Robinson, I.M. Torrens, Phys. Rev. B 9 (1974) 5008.
[38] J. Lindhard, J.V. Niesen, M. Scharff, Mat. Fys. Medd. Dan. Vidensk. Selsk. 36 (10) (1968) 1.